NANO LETTERS

Letter

pubs.acs.org/NanoLett

Controlling Subnanometer Gaps in Plasmonic Dimers Using Graphene

Jan Mertens,[†] Anna L. Eiden,[†,‡] Daniel O. Sigle,[†] Fumin Huang,[†] Antonio Lombardo,[‡] Zhipei Sun,[‡] Ravi S. Sundaram,[‡] Alan Colli,[§] Christos Tserkezis,[∥] Javier Aizpurua,[∥] Silvia Milana,[‡] Andrea C. Ferrari,[‡] and Jeremy J. Baumberg*[,†]

[†]NanoPhotonics Centre, Cavendish Laboratory, University of Cambridge, Cambridge, CB3 0HE, United Kingdom

[‡]Cambridge Graphene Centre, University of Cambridge, 9 JJ Thomson Avenue, Cambridge CB3 0FA, United Kingdom

[§]Nokia Research Center, Broers Building, Cambridge CB3 0FA, United Kingdom

[∥]Materials Physics Center CSIC-UPV/EHU and DIPC, Paseo Manuel de Lardizabal 5, 20018 Donostia-San Sebastián, Spain

S *Supporting Information*

ABSTRACT: Graphene is used as the thinnest possible spacer between gold nanoparticles and a gold substrate. This creates a robust, repeatable, and stable subnanometer gap for massive plasmonic field enhancements. White light spectroscopy of single 80 nm gold nanoparticles reveals plasmonic coupling between the particle and its image within the gold substrate. While for a single graphene layer, spectral doublets from coupled dimer modes are observed shifted into the near-infrared, these disappear for increasing numbers of layers. These doublets arise from charger-transfer-sensitive gap plasmons, allowing optical measurement to access out-of-plane conductivity in such layered systems. Gating the graphene can thus directly produce plasmon tuning.

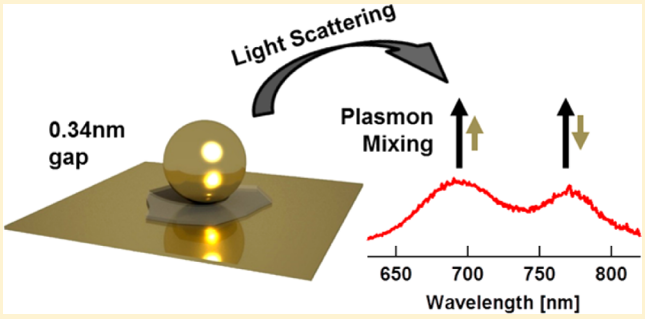

KEYWORDS: *Localized plasmons, dimer, graphene, field enhancement, nanoparticle*

Precise separation of plasmonic nanostructures is of widespread interest, because it controls the build-up of intense and localized optical fields, as well as their spectral tuning.[1,2] Surface-enhanced Raman scattering relies on this plasmonic enhancement to enable identification of trace molecules captured within such gaps, down to femtomolar levels.[3−8] Plasmonic enhancement can also be used to improve the efficiency of photodetectors.[9] Similarly, nonlinear frequency conversion depends critically on the field enhancements, their spatial localization, and their spectral resonances, all of which depend ultrasensitively on the plasmonic gaps.[10] On the other hand fundamental processes like quantum tunnelling can be observed optically, but only for gap separations in the subnanometre regime.[11]

It is a major challenge to separate nanostructures precisely in the subnanometre regime because of poor structural control achievable on such length scales. Here we use a single layer of graphene (SLG) as a precise spacer between gold nanoparticles (AuNPs) and a Au surface to create stable subnanometre gaps down to 0.34 nm. This provides an optical probe of conductivity perpendicular to the graphene sheet, as well as a means to tune the plasmonic resonances by precise separation of NPs from the Au surface using flakes with increasing number of layers (N). Scattering from AuNPs placed directly on Au is compared with that of AuNPs separated from the Au substrate by flakes with increasing N. Splitting of the coupled plasmonic mode into a spectral doublet is observed due to gap plasmons controlled by the SLG. Wide tuning of plasmonic resonances can thus become possible by modulating the graphene dielectric response, for instance, using gates. Such a robust nanoparticle-on-layered-material configuration forms a versatile platform for investigating a wide variety of plasmonic and monolayer functionalities and devices.

In our experiments, a polished silicon substrate is coated with a 100 nm Au film deposited by electron beam evaporation (Figure 1a). Graphene is prepared either via micromechanical cleavage of graphite or by chemical vapor deposition (CVD).[12,13] The number of layers N is determined by a combination of Raman spectroscopy[14,15] and optical microscopy.[16,17] Raman spectroscopy is also used to monitor the structural quality and doping of the graphene layers throughout the transfer process.[14,15] Graphene is then transferred onto the Au film. Transfer of CVD graphene is performed as follows:[12,13] the initial SLG deposited on Cu is spin-coated with a thin layer of poly(methyl methacrylate) (PMMA). Cu is then dissolved in a 3% H_2O_2/35% HCl (3:1 ratio) mixture,

Received: May 20, 2013
Revised: August 26, 2013
Published: September 24, 2013

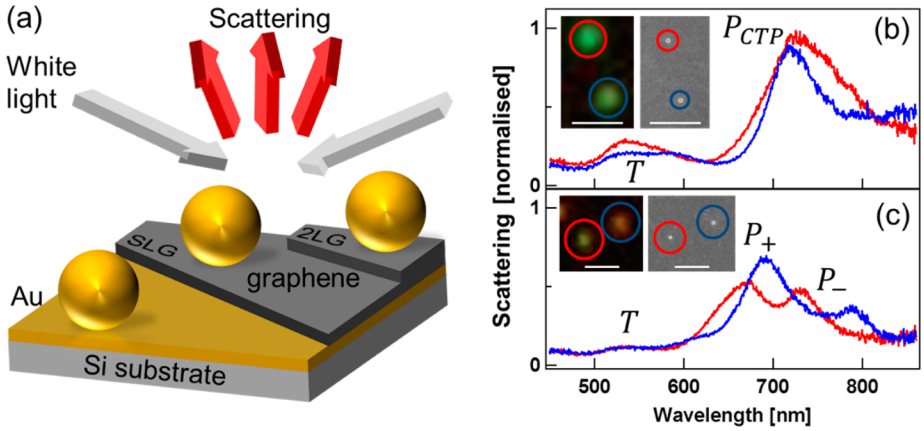

Figure 1. (a) Schematic of experiment. Graphene placed on a thick Au substrate, with 80 nm AuNPs deposited on top. Incident white light at high angles is scattered into the detector. (b,c) Dark-field single particle scattering spectra for (b) two AuNPs in direct contact with Au substrate, and (c) two AuNPs on CVD-grown monolayer graphene transferred onto Au. Insets show (left) dark-field images and (right) SEM images of same NPs. Scale bar is 1 μm.

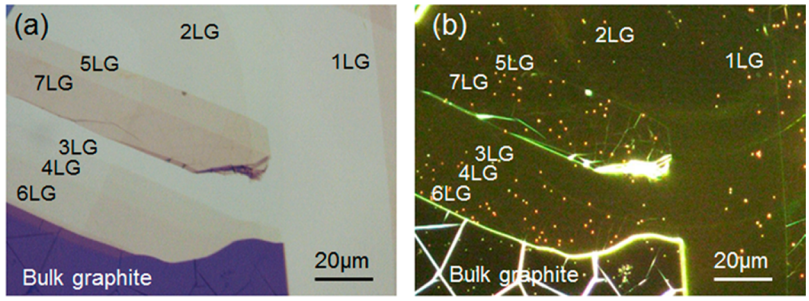

Figure 2. Exfoliated graphene on Au film. The number of graphene layers is indicated. (a) Bright-field image before AuNP transfer. (b) Dark-field scattering of the same area after AuNPs are transferred onto the graphene flakes.

further diluted in an equal volume of deionized water. After all the Cu is dissolved, the remaining PMMA/graphene film is placed on the Au film, and PMMA is finally removed with acetone. Mechanically exfoliated graphene is transferred as follows:[12] Three layers of 950 K PMMA are spin coated on the Si/SiO_2 substrates where flakes are deposited. The samples are subsequently immersed in deionized water at 90 °C for 2 h, resulting in the detachment of the polymer film due to the intercalation of water at the polymer−SiO_2 interface. Graphene flakes stick to the PMMA film and can thus be removed from the original substrate. The PMMA/graphene film is then transferred onto the Au substrate. Because a thin layer of water is trapped at the substrate−polymer interface, the latter can be moved across the target substrate allowing accurate positioning of a chosen graphene flake onto a specific location on the Au substrate. The sample is then left to dry, and finally PMMA is dissolved by acetone drop casting followed by immersion, resulting in the gentle release of the selected graphene flake on the Au substrate.

Near-spherical 80 nm AuNPs (BBI, citrate stabilized) are then self-assembled on a polished Si substrate treated with (3-aminopropyl)-triethoxysilane (APTES). The substrate is first dipped into a solution of 80 nm AuNPs for 30 s and then rinsed in deionized water to remove remaining unbound colloidal NPs. The self-assembled NPs are then transferred from the silicon substrate onto the graphene using the same PMMA transfer method previously described for the exfoliated graphene transfer. Since the citrate-stabilized AuNPs are not surrounded by ligands, the spacing between Au surface and AuNP is well-defined by the graphene.

We characterize the scattering of white light from single AuNPs on the sample in areas that are covered with graphene flakes of increasing N. Single particles are identified using dark-field microscopy. Unpolarized light from an incandescent source is focused on the sample using a 100× objective with a numerical aperture of 0.85 so that the sample is uniformly illuminated from large angles of incidence. The scattered light is detected with both a charge-coupled device (CCD) camera and also collected with a multimode optical fiber attached to a cooled spectrometer. The fiber has a core diameter of 50 μm to give a collection spot with a diameter of ≃500 nm. Precise positioning of the AuNPs in the collection area is achieved using piezoelectric translation stages. The same AuNPs are also examined in a scanning electron microscope (SEM) to identify their shape. Direct correlation between SEM images and dark-field spectra is necessary to correctly interpret the scattering spectra, since these depend strongly on the particle shape.

Dark-field scattering spectra of four individual 80 nm AuNPs are shown in Figure 1b,c. The insets of these graphs show dark-field images (left) and SEM images (right) of the same AuNPs that are seen to be near-spherical. When the AuNPs directly contact the Au substrate (Figure 1b) two scattering modes, T and P_{CTP}, are clearly visible for each particle with resonance wavelengths of 530 nm and 720 nm, respectively. The intensity of mode P_{CTP} is stronger than T (even accounting for chromatic aberration, which gives each mode a different optimal focus). In contrast, when the AuNPs are separated

dx.doi.org/10.1021/nl4018463 | Nano Lett. 2013, 13, 5033−5038

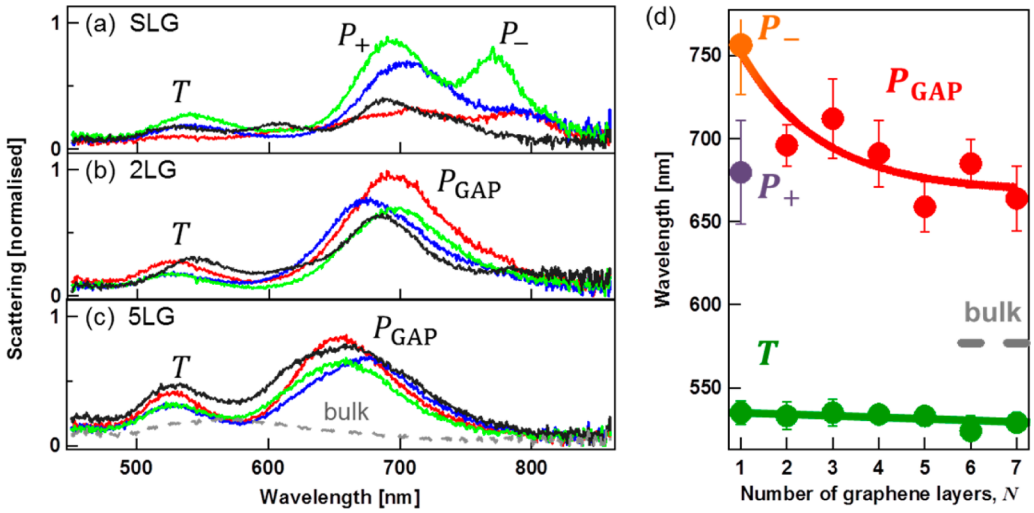

Figure 3. (a–c) Dark-field single particle scattering spectra of four AuNPs on SLG, 2LG, and 5LG. Dashed gray curve (bottom graph) is scattering from AuNP on bulk graphite. (d) Resonance wavelength (averaged over many AuNPs, variance given by the error bars) of the plasmonic T, P_+, P_-, and P_{GAP} modes for increasing N.

from the Au film by a CVD grown graphene monolayer three resonances are observed (Figure 1c). The resonance wavelength of the short wavelength mode T is unaffected by the SLG spacer, however in the near-infrared region two modes P_+ and P_- are detected. While the absolute spectral positions of the two modes for the two particles are not exactly the same, their spectral separation is comparable. Similar infrared spectral doublets are seen for all spherical AuNPs.

As we discuss below, this doublet arises from the coupling of the normal dipolar plasmon across the AuNP and its image with a gap plasmon highly localized in the SLG area directly underneath the NP. To prove this, we examine the dependence of the spectra on N. The AuNPs on top of the flakes are seen as bright spots in dark field images (Figure 2), and already show visibly the coupling effects since the AuNP spots on top of bulk graphite are spectrally shifted into the green compared to their red appearance in the regions of 1–6 layers of graphene (LG). Figure 3a shows that the spectral doublet is only seen for the SLG spacer, while the infrared mode blueshifts with increasing N (Figure 3b,c). We emphasize that the spectral doublet when using a SLG spacer does not depend on how graphene is prepared (i.e., CVD or micromechanical exfoliation) and is reproducible across many AuNPs. While the spectra show some variability (±50 nm) in the absolute spectral position of the resonance peaks for small N, they become rather stable for $N >$ 3. This is expected from the extreme sensitivity of the plasmonic modes in the gap to the precise dielectric environment (for instance water).

To understand the origin of the doublet, we first show schematically the spectral evolution of the different plasmon modes associated with AuNPs on Au substrates spaced by conducting gaps (Figure 4a). This tuning map is based on experimental[18,19] and theoretical[20,21] studies of plasmons in NP dimers. While dimers are hard to fabricate reliably, the NP-on-substrate geometry here produces an equivalent (but robust) system since solutions of the electromagnetic boundary conditions at the planar surface are equivalent to an image NP inside the metal. The NP sees its reflection in the mirror and couples to it, so that each charged region produces a dipole in conjunction with the oppositely charged image NP.

When the optical field is polarized in the plane of the substrate, it excites transverse plasmons across the AuNP (T) that are spaced far enough above the surface to produce only a weak coupling (Figure 4b(i)) and a resonance close to that of individual AuNPs.[22,23] Two other types of dipoles are driven by the component of the optical field along the dimer axis (excited by the high-angle incident light). One of these is the dipole resonance of the whole system, arising from the electric polarization between the charge in the main body of the AuNP and its equal and opposite charge in the image NP. This global dipole plasmon (long arrows in Figure 4b, P_{CTP}) is present whenever the gap conducts and is the charge-transfer plasmon (CTP). The other dipole is located in the immediate vicinity of the gap (hence we term it the "GAP plasmon"). This latter dipole (small arrows in Figure 4b, P_{GAP}) has a much smaller cross-section, since it is highly localized, and is extremely sensitive to the gap. These two longitudinal (CTP and GAP) plasmons couple to each other to produce mixtures (Figure 4b(ii,iii)) in which they are aligned either parallel ($P_+ = P_{CTP} + P_{GAP}$) or antiparallel ($P_- = P_{CTP} - P_{GAP}$) in a form of plasmon hybridization closely analogous to ferromagnetic and antiferromagnetic dipolar coupling.[24] While the P_- mode is dipolar-like, the P_+ mode is more quadrupolar due to the different lateral distributions of charge in the CTP and GAP dipoles (see Supporting Information). The strength of this coupling between CTP and GAP dipoles sets the splitting between the doublet states and is controlled predominantly by the strength of the gap dipole. While bright and dark plasmonic modes have been observed in conductive gap systems,[25] dark plasmons can only be studied with localized probes such as electron beams in electron energy loss spectroscopy.[26] Furthermore, asymmetric dark modes are not supported by the highly symmetric NP-on-surface geometry and are not the origin of the splitting observed here.[27]

The resonant wavelengths of the longitudinal plasmonic modes (Figure 4a, red lines) shift with gap separation and/or conductivity of the junction. Two main regimes are observed: the touching regime (left side), and the nontouching regime (right side), separated by a quantum mechanical tunnelling regime for angstrom-scale gaps (labeled QM).[11,20,21] In the touching regime, the junction conductivity is high, thus charge

dx.doi.org/10.1021/nl4018463 | Nano Lett. 2013, 13, 5033–5038

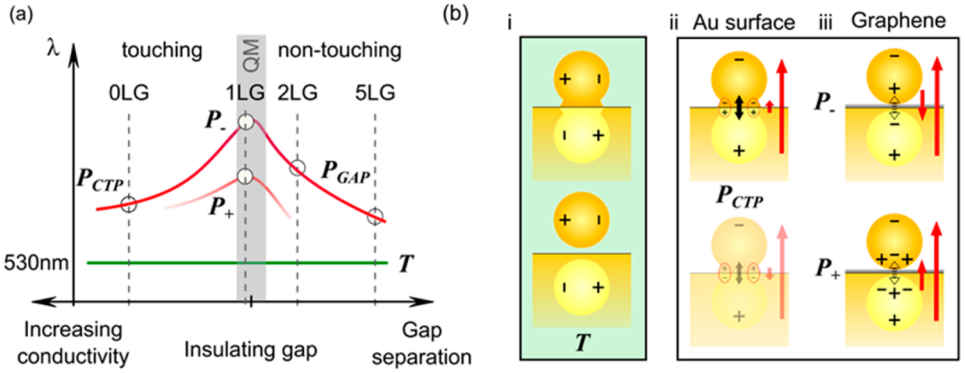

Figure 4. (a) Schematic spectral evolution of plasmon modes for AuNPs on Au with conducting gaps of different resistivity. Experimental data are labeled with the spacer thickness, indicated by the number of graphene layers (0−5LG). (b) Plasmonic charge distributions for AuNPs in contact with Au surface (i,ii) and when a SLG spacer is present (iii). Red arrows indicate induced dipole orientation and strength.

can rapidly move between the AuNP underside and the Au film. This shorts out most of the dipole in the gap plasmon, leaving a single CTP plasmon. In the nontouching regime, this charge transfer cannot occur, and the tuning and splitting of the two modes is set by the decreasing strength of the gap plasmon as the Au surfaces move further apart. The transverse modes (green lines) are not affected by the coupling, as expected from their charge distribution and consistent with our experimental observations (Figure 3d). Note that although the gap plasmon has a smaller cross section than the global dipole, locally this gap plasmon can give rise to very large local fields of interest in field-enhanced spectroscopies.

The red curves show that the energy splitting between P_+ and P_- is only seen when the gap is small (enhancing the gap plasmon cross section), and the junction is weakly conducting (avoiding discharging the gap plasmon). With no graphene in the gap, the Au atoms in the NP touching the Au film rearrange to form a significant neck (Figure 4b(i)) with high conductivity. Such ductile necking between AuNPs is well-known[28−30] and supported by our theoretical model (Supporting Information) that indicates that the spectrum observed cannot arise for a perfect sphere resting on a plane. When a SLG spacer is used, the vertical resistance is sufficient to prevent discharge of the gap plasmon and both parallel and antiparallel modes are seen. Our theoretical models using literature values for the graphene dielectric constant[31,32] show indeed that only a SLG spacer produces a doublet resonance (see Supporting Information). This confirms that the experimental gap width for the SLG spacer is consistent with the pure 0.34 nm SLG thickness. Increasing N increases both the resistance (linearly with N) and also the gap width (which near-exponentially decreases the gap plasmon strength). Hence the dominant effect is to collapse the doublet and blueshift the gap plasmon. This is clearly seen in Figure 3d, and marked as points 0−5LG on Figure 4a.

The SLG thus acts in two ways. It forms a robust and perfectly controlled 0.34 nm gap spacer between the Au substrate and AuNP with a high resistance compared to that needed to discharge the gap plasmon within half an optical cycle (1.5 fs). However, it also prevents the wetting of AuNPs on the substrate, preserving their distinct near-spherical morphology on the nonwetting SLG.[33,34] Au has a low adsorption on graphene so that the contact area of AuNPs on SLG is reduced compared to the direct contact of AuNPs on Au surfaces.[34,35] A "digital" spacing step of 0.34 nm is produced using flakes of increasing N,[16] allowing this geometry to be used as a test-bed for many plasmonic predictions as well as device functions.

The spectral separation of the doublet is sensitive to the gap width and vertical resistance through the SLG. Exact calculations of the charge transport from Au through SLG and back into Au require combinations of coupled Schrödinger-Poisson equations with electromagnetism.[11,21] Vertical transport through a metal/SLG/metal structure can occur either via direct metal-to-metal tunnelling or via the graphene itself. Recent work[36,37] supports the direct tunnelling model and reports vertical resistivities at low voltages of $\sim 5 \times 10^{-4}$ Ω cm^2 (at room temperature). For comparison, studies of tunnelling through metal/vacuum/metal systems using the Simmons formula[38] in the low-voltage approximation report tunnelling resistivities for a 0.3−0.4 nm gap on the order of 10^{-3} Ω cm^2 or lower.[39−41] On the other hand, if transport occurs through graphene, a crude estimate of the vertical resistivity can be made from the interlayer resistance in graphite, or from the average metal/graphene contact resistance in planar graphene devices. A realistic range would span from 10^{-3} down to 10^{-6} Ω cm^2 for certain metals.[42,43] This range overlaps with estimates for the direct tunnelling above and also with the value reported by ref 36. The different spectral positions and separations of the doublets seen in Figures 1 and 3 result from this strong sensitivity to the transport in this local environment. The spectral response to light thus becomes a way to characterize the local vertical conductivity in graphene and in other two-dimensional crystals obtained from the exfoliation of layered materials such as MoS_2, WS_2, BN, and so forth,[13] as well as other semiconductors or more complex multilayer stacks. The enhanced local fields can already be seen in the surface-enhanced Raman scattering of the graphene in these gaps, which is enhanced by over 2 orders of magnitude for 633 nm excitation, and over 3 orders of magnitude for 785 nm excitation (see Supporting Information). Given that the Raman laser spot size is 1 μm in diameter, and the lateral width of the P_+ mode given by theory is 8 nm (see Supporting Information), this implies local Raman enhancements of greater than 10^7. Such large values offer opportunities for enhancing graphene-based photodetectors.[9]

In conclusion, we have shown that graphene acts as an ideal spacer for plasmonic nanostructures. In this NP-atomic layer-substrate configuration, graphene produces a stable and precise subnanometer separation of AuNPs from a Au surface and prevents coagulation of AuNPs with the Au substrate. A spectral doublet of the coupled plasmon resonance is observed

dx.doi.org/10.1021/nl4018463 | Nano Lett. 2013, 13, 5033−5038

in the near-infrared when NPs are separated from the Au substrate by a graphene monolayer. This doublet resonance corresponds to coupling between charge-transfer and gap plasmons mixed in parallel and antiparallel configurations. The spectral position of the resonances depends on the resistivity of the junction between the NP and Au surface as well as on the gap size, and strong shifts are observed with increasing numbers of layers. This work opens up the prospect for wide tuning of plasmonic resonances by modulating the graphene dielectric response, for instance, using gates.

■ ASSOCIATED CONTENT

Supporting Information

Raman measurements, together with field profiles. This material is available free of charge via the Internet at http://pubs.acs.org.

■ AUTHOR INFORMATION

Corresponding Author

*E-mail: jjb12@cam.ac.uk.

Notes

The authors declare no competing financial interest.

■ ACKNOWLEDGMENTS

We gratefully acknowledge support from U.K. EPSRC Grants EP/G060649/1, EP/G037221/1, EP/H007024/1, EP/G042357/1, EP/K01711X/1, EP/K017144/1, from ERC Grants LINASS 320503 and NANOPOTS, from Nokia Research Centre, and from a Royal Society Wolfson Research Merit Award, EU Grants RODIN, GENIUS, CareRAMM, Graphene Flagship (contract no. CNECT-ICT-604391), Project FIS2010-19609-C02-01 of the Spanish Ministry of Science and Education and project IT756-13 of the Basque Government for groups in the UPV/EHU. J.M. acknowledges support from the Winton Programme of the Physics of Sustainability.

■ REFERENCES

(1) Ciracì, C.; Hill, R. T.; Mock, J. J.; Urzhumov, Y.; Fernández-Domínguez, A. I.; Maier, S. A.; Pendry, J. B.; Chilkoti, A.; Smith, D. R. Probing the Ultimate Limits of Plasmonic Enhancement. *Science* **2012**, *337* (6098), 1072−1074.

(2) Moreau, A.; Ciraci, C.; Mock, J. J.; Hill, R. T.; Wang, Q.; Wiley, B. J.; Chilkoti, A.; Smith, D. R. Controlled-reflectance surfaces with film-coupled colloidal nanoantennas. *Nature* **2012**, *492* (7427), 86−89.

(3) Fleischmann, M.; Hendra, P. J.; McQuillan, A. J. Raman spectra of pyridine adsorbed at a silver electrode. *Chem. Phys. Lett.* **1974**, *26* (2), 163−166.

(4) Kneipp, K.; Wang, Y.; Kneipp, H.; Perelman, L. T.; Itzkan, I.; Dasari, R. R.; Feld, M. S. Single Molecule Detection Using Surface-Enhanced Raman Scattering (SERS). *Phys. Rev. Lett.* **1997**, *78* (9), 1667−1670.

(5) Kneipp, K.; Kneipp, H.; Itzkan, I.; Dasari, R. R.; Feld, M. S. Surface-enhanced Raman scattering and biophysics. *J. Phys.: Condens. Matter* **2002**, *14* (18), R597.

(6) Le Ru, E. C.; Etchegoin, P. G. Sub-wavelength localization of hot-spots in SERS. *Chem. Phys. Lett.* **2004**, *396* (4−6), 393−397.

(7) Jensen, L.; Aikens, C. M.; Schatz, G. C. Electronic structure methods for studying surface-enhanced Raman scattering. *Chem. Soc. Rev.* **2008**, *37* (5), 1061−1073.

(8) Nie, S.; Emory, S. R. Probing Single Molecules and Single Nanoparticles by Surface-Enhanced Raman Scattering. *Science* **1997**, *275* (5303), 1102−1106.

(9) Echtermeyer, T. J.; Britnell, L.; Jasnos, P. K.; Lombardo, A.; Gorbachev, R. V.; Grigorenko, A. N.; Geim, A. K.; Ferrari, A. C.; Novoselov, K. S. Strong plasmonic enhancement of photovoltage in graphene. *Nat. Commun.* **2011**, *2*, 458.

(10) Zhang, Y.; Grady, N. K.; Ayala-Orozco, C.; Halas, N. J. Three-Dimensional Nanostructures as Highly Efficient Generators of Second Harmonic Light. *Nano Lett.* **2011**, *11* (12), 5519−5523.

(11) Savage, K. J.; Hawkeye, M. M.; Esteban, R.; Borisov, A. G.; Aizpurua, J.; Baumberg, J. J. Revealing the quantum regime in tunnelling plasmonics. *Nature* **2012**, *491* (7425), 574−577.

(12) Bae, S.; Kim, H.; Lee, Y.; Xu, X.; Park, J.-S.; Zheng, Y.; Balakrishnan, J.; Lei, T.; Ri Kim, H.; Song, Y. I.; Kim, Y.-J.; Kim, K. S.; Ozyilmaz, B.; Ahn, J.-H.; Hong, B. H.; Iijima, S. Roll-to-roll production of 30-inch graphene films for transparent electrodes. *Nat. Nanotechnol* **2010**, *5* (8), 574−578.

(13) Bonaccorso, F.; Lombardo, A.; Hasan, T.; Sun, Z.; Colombo, L.; Ferrari, A. C. Production and processing of graphene and 2d crystals. *Mater. Today* **2012**, *15* (12), 564−589.

(14) Ferrari, A. C.; Meyer, J. C.; Scardaci, V.; Casiraghi, C.; Lazzeri, M.; Mauri, F.; Piscanec, S.; Jiang, D.; Novoselov, K. S.; Roth, S.; Geim, A. K. Raman Spectrum of Graphene and Graphene Layers. *Phys. Rev. Lett.* **2006**, *97* (18), 187401.

(15) Ferrari, A. C.; Basko, D. M. Raman spectroscopy as a versatile tool for studying the properties of graphene. *Nat. Nanotechnol.* **2013**, *8* (4), 235−246.

(16) Blake, P.; Hill, E. W.; Neto, A. H. C.; Novoselov, K. S.; Jiang, D.; Yang, R.; Booth, T. J.; Geim, A. K. Making graphene visible. *Appl. Phys. Lett.* **2007**, *91* (6), 063124.

(17) Casiraghi, C.; Hartschuh, A.; Lidorikis, E.; Qian, H.; Harutyunyan, H.; Gokus, T.; Novoselov, K. S.; Ferrari, A. C. Rayleigh Imaging of Graphene and Graphene Layers. *Nano Lett.* **2007**, *7* (9), 2711−2717.

(18) Atay, T.; Song, J.-H.; Nurmikko, A. V. Strongly Interacting Plasmon Nanoparticle Pairs: From Dipole−Dipole Interaction to Conductively Coupled Regime. *Nano Lett.* **2004**, *4* (9), 1627−1631.

(19) Scholl, J. A.; García-Etxarri, A.; Koh, A. L.; Dionne, J. A. Observation of Quantum Tunneling between Two Plasmonic Nanoparticles. *Nano Lett.* **2012**, *13* (2), 564−569.

(20) Romero, I.; Aizpurua, J.; Bryant, G. W.; García De Abajo, F. J. Plasmons in nearly touching metallic nanoparticles: singular response in the limit of touching dimers. *Opt. Express* **2006**, *14* (21), 9988−9999.

(21) Esteban, R.; Borisov, A. G.; Nordlander, P.; Aizpurua, J. Bridging quantum and classical plasmonics with a quantum-corrected model. *Nat. Commun.* **2012**, *3*, 825.

(22) Okamoto, T.; Yamaguchi, I. Optical Absorption Study of the Surface Plasmon Resonance in Gold Nanoparticles Immobilized onto a Gold Substrate by Self-Assembly Technique. *J. Phys. Chem. B* **2003**, *107* (38), 10321−10324.

(23) Chen, S.-Y.; Mock, J. J.; Hill, R. T.; Chilkoti, A.; Smith, D. R.; Lazarides, A. A. Gold Nanoparticles on Polarizable Surfaces as Raman Scattering Antennas. *ACS Nano* **2010**, *4* (11), 6535−6546.

(24) We note alternative terminologies also in use. For conducting gaps, the P_+ mode is termed the charge-transfer mode 1, and P_- is termed the charge-transfer mode 2. In the insulating gap case, the gap plasmon mode is termed the bonding dipole plasmon (BDP).

(25) Duan, H.; Fernández-Domínguez, A. I.; Bosman, M.; Maier, S. A.; Yang, J. K. W. Nanoplasmonics: Classical down to the Nanometer Scale. *Nano Lett.* **2012**, *12* (3), 1683−1689.

(26) Chu, M.-W.; Myroshnychenko, V.; Chen, C. H.; Deng, J.-P.; Mou, C.-Y.; García de Abajo, F. J. Probing Bright and Dark Surface-Plasmon Modes in Individual and Coupled Noble Metal Nanoparticles Using an Electron Beam. *Nano Lett.* **2008**, *9* (1), 399−404.

(27) Yamamoto, N.; Ohtani, S.; García de Abajo, F. J. Gap and Mie Plasmons in Individual Silver Nanospheres near a Silver Surface. *Nano Lett.* **2010**, *11* (1), 91−95.

(28) Arcidiacono, S.; Bieri, N. R.; Poulikakos, D.; Grigoropoulos, C. P. On the coalescence of gold nanoparticles. *Int. J. Multiphase Flow* **2004**, *30* (7−8), 979−994.

(29) Zhang, R.; Hummelgård, M.; Olin, H. Single layer porous gold films grown at different temperatures. *Physica B* **2010**, *405* (21), 4517−4522.
(30) Pérez-González, O.; Zabala, N.; Borisov, A. G.; Halas, N. J.; Nordlander, P.; Aizpurua, J. Optical Spectroscopy of Conductive Junctions in Plasmonic Cavities. *Nano Lett.* **2010**, *10* (8), 3090−3095.
(31) Lidorikis, E.; Ferrari, A. C. Photonics with Multiwall Carbon Nanotube Arrays. *ACS Nano* **2009**, *3* (5), 1238−1248.
(32) Bruna, M.; Vaira, A.; Battiato, A.; Vittone, E.; Borini, S. Graphene strain tuning by control of the substrate surface chemistry. *Appl. Phys. Lett.* **2010**, *97* (2), 021911.
(33) Schedin, F.; Lidorikis, E.; Lombardo, A.; Kravets, V. G.; Geim, A. K.; Grigorenko, A. N.; Novoselov, K. S.; Ferrari, A. C. Surface-Enhanced Raman Spectroscopy of Graphene. *ACS Nano* **2010**, *4* (10), 5617−5626.
(34) Zan, R.; Bangert, U.; Ramasse, Q.; Novoselov, K. S. Metal−Graphene Interaction Studied via Atomic Resolution Scanning Transmission Electron Microscopy. *Nano Lett.* **2011**, *11* (3), 1087−1092.
(35) Gong, C.; Hinojos, D.; Wang, W.; Nijem, N.; Shan, B.; Wallace, R. M.; Cho, K.; Chabal, Y. J. Metal−Graphene−Metal Sandwich Contacts for Enhanced Interface Bonding and Work Function Control. *ACS Nano* **2012**, *6* (6), 5381−5387.
(36) Cobas, E.; Friedman, A. L.; van't Erve, O. M. J.; Robinson, J. T.; Jonker, B. T. Graphene As a Tunnel Barrier: Graphene-Based Magnetic Tunnel Junctions. *Nano Lett.* **2012**, *12* (6), 3000−3004.
(37) Lee, Y.-H.; Kim, Y.-J.; Lee, J.-H. Vertical conduction behavior through atomic graphene device under transverse electric field. *Appl. Phys. Lett.* **2011**, *98* (13), 133112.
(38) Simmons, J. G. Generalized Formula for the Electric Tunnel Effect between Similar Electrodes Separated by a Thin Insulating Film. *J. Appl. Phys.* **1963**, *34* (6), 1793−1803.
(39) Young, R.; Ward, J.; Scire, F. Observation of Metal-Vacuum-Metal Tunneling, Field Emission, and the Transition Region. *Phys. Rev. Lett.* **1971**, *27* (14), 922−924.
(40) Teague, E. C. Room Temperature Gold-Vacuum-Gold Tunneling Experiments. *J. Res. Natl. Bur. Stand.* **1986**, *91*, 171−233.
(41) Bryant, P. J.; Kim, H. S.; Yang, R.; Zheng, Y. C.; Miller, R. Current-voltage characteristics of metal/vacuum/metal tunneling. *J. Vac. Sci. Technol., A* **1988**, *6* (2), 534−536.
(42) Nagashio, K.; Nishimura, T.; Kita, K.; Toriumi, A. Contact resistivity and current flow path at metal/graphene contact. *Appl. Phys. Lett.* **2010**, *97* (14), 143514−143514−3.
(43) Do, V. N.; Anh Le, H. Transport characteristics of graphene-metal interfaces. *Appl. Phys. Lett.* **2012**, *101* (16), 161605.